Reproduced from Soil Science Society of America Journal. Published by Soil Science Society of America. All copyrights reserved.

DIVISION S-9—SOIL MINERALOGY

Clay Mineralogical Transformations over Time in Hanford Sediments Reacted with Simulated Tank Waste

Kholoud Mashal, James B. Harsh, and Markus Flury*

ABSTRACT

Buried waste storage tanks at the USDOE Hanford Reservation in Washington State have released solutions containing high concentrations of Na, OH, NO_3, and Al into the vadose zone. When such solutions contact vadose zone sediments, mineral transformations will change the sediment matrix. We hypothesized that Si, dissolved from primary and secondary minerals, will combine with Al from the tank waste to form crystalline or poorly crystalline network silicates such as zeolites and feldspathoids. In this study, we characterized the colloidal (<2 μm equivalent diam.) minerals formed when simulated tank solutions reacted with vadose zone Hanford sediments. Variables studied included simulated tank waste (STW) composition, reaction time, and temperature. Hanford sediments were reacted with a series of simulated tank solutions in batch experiments at 25 and 50°C for 1, 10, 25, 40, and 50 d. The mineralogical, structural, and chemical properties of the resulting colloidal fractions and bulk solutions were determined by x-ray diffraction (XRD), Fourier transform infrared (FTIR), ^{27}Al- and ^{29}Si-magic angle spinning-nuclear magnetic resonance (MAS-NMR), scanning electron microscopy (SEM), energy-dispersive x-ray analysis (EDAX), colorimetry, atomic absorption spectroscopy, and inductively coupled plasma–atomic emission spectroscopy (ICP–AES). Upon contact with STW, Si was released from the sediments and a portion was incorporated into poorly crystalline solids. The amount of poorly crystalline solids increased initially and reached maximum quantities between 0 and 25 d. Lability of minerals in the presence of NaOH followed the order quartz → kaolinite → illite. New secondary minerals, NO_3–cancrinite, NO_3–sodalite, and zeolite A, were formed at the expense of the original clay minerals. Zeolite A was labile and disappeared after about 25 d of reaction time. Cancrinite and sodalite, however, appeared to be stable and increased in abundance with time.

Aqueous high-level radioactive wastes have been produced as a byproduct of Pu production at the Hanford nuclear site in Washington state. The high-level waste was stored in 177 steel-lined underground tanks and has an estimated volume of about 65 million gallons (Gephart and Lundgren, 1998). These wastes are alkaline and high in ionic strength. The composition of the waste includes radionuclides and high concentrations of NaOH, $NaNO_2$, $NaNO_3$, and $NaAlO_2$ (Serne et al., 1998). Following leakage of the tanks, the heat generated by radioactive decay resulted in temperatures beneath the tank in excess of 50°C (Pruess et al., 2002).

When highly alkaline solutions contact clay minerals, mineral dissolution and precipitation may occur. The effect of alkaline solutions on the transformation of clay minerals has been the subject of intensive research (Cuadros and Linares, 1996; Bauer and Berger, 1998; Bauer and Velde, 1999; Taubald et al., 2000). Bauer and coworkers (1998, 1999) studied the reaction of kaolinite in KOH solutions and reported the formation of new solid phases. Buhl et al. (1997) found that kaolinite was transformed to sodalite at pH > 10. Upon the reaction of kaolinite with a NaOH-$NaNO_3$ mixture, the following mineral transformation sequence was found: kaolinite → fly ash → montmorillonite → natural zeolite (Park et al., 2000).

Many studies have been conducted on the transformation of aluminosilicates at high pH, but few reports are available on the type of minerals that could form in situ under the leaking Hanford waste tanks. Hanford sediments consist of primary phases such as quartz and feldspars and secondary phases such as aluminosilicate clays and iron oxides (Serne et al., 2002). Recently, minerals representative of Hanford sediments were subject to mineral transformation studies. For example, when quartz was reacted with STWs, NO_3–cancrinite was found to precipitate on the quartz surface (Bickmore et al., 2001). Chorover et al. (2003) examined the dissolution of kaolinite reacted with STW and reported the formation of network aluminosilicates, including zeolite (chabazite), NO_3–cancrinite, and NO_3–sodalite. Zhao et al. (2004) corroborated these results, finding that both cancrinite and sodalite formed when kaolinite reacted with STWs.

Similar reactions occurred when Hanford sediments reacted with STWs at elevated temperatures (60–90°C) where silicate minerals dissolved and zeolitic phases precipitated (Kaplan et al., 1998; Nyman et al., 2000; Qafoku et al., 2003a, 2004; Mashal et al., 2004). The mineral dissolution rates and the morphology of the secondary precipitates were found to be dependent on Si/Al aqueous molar ratios (Qafoku et al., 2003a). In another study, STWs in contact with Hanford sediments precipitated cancrinite and sodalite in the colloidal size fraction (Mashal et al., 2004).

Here, we want to expand the existing knowledge of colloidal material formed in Hanford sediments reacted with STW. The objective of this work was to investigate and characterize the colloidal materials (<2 μm in

Dep. of Crop and Soil Sciences, Center for Multiphase Environmental Research, Washington State Univ., Pullman, WA 99164-6420. Received 5 July 2004. *Corresponding author (flury@mail.wsu.edu).

Published in Soil Sci. Soc. Am. J. 69:531–538 (2005).
© Soil Science Society of America
677 S. Segoe Rd., Madison, WI 53711 USA

Abbreviations: AAO, acidic ammonium oxalate; AES, atomic emission spectroscopy; EDAX, energy-dispersive x-ray analysis; FTIR, Fourier transform infrared; ICP, inductively coupled plasma; MAS, magic angle spinning; NCA, noncarbonate alkalinity; SEM, scanning electron microscopy; STW, simulated tank waste; XRD, x-ray diffraction.

Reproduced from Soil Science Society of America Journal. Published by Soil Science Society of America. All copyrights reserved.

diam.) resulting from Hanford sediments reacted with STWs with varying NaOH, $NaNO_3$, and $NaAlO_4$ concentrations and temperatures (25 and 50°C). We focus on colloidal material because of its potential role in the facilitation of contaminant transport.

MATERIALS AND METHODS

Sediments and Simulated Tank Waste Solutions

The sediments used in this study were obtained from the Hanford Reservation, Richland, WA. Sediment characterization is described in detail elsewhere (Serne et al., 2002; Mashal et al., 2004). Uncontaminated sediments were collected from the submarine pit (218-E-12B) at the Hanford site and are considered representative for the material underlying the S-SX (single-shell) tank farm at Hanford (personal communication, September 2001, Bruce N. Bjornstad, Pacific Northwest National Laboratories, Richland, WA). The sediments were air dried and sieved through a 2-mm square screen.

The colloidal fraction (equivalent diam. < 2 μm) of the sediments was separated using gravity sedimentation. For that purpose, sediments were dispersed in a solution containing 0.5 g L^{-1} Na-hexametaphosphate. The suspension was kept in a 1-L volumetric cylinder and the suspension height was 30 cm. The particles were left to settle for 24 h. According to Stokes law, particles with equivalent diam. < 2 μm should remain in suspension after that time. The suspension was then decanted and used for the colloidal material retained for further characterization.

We used different STW solutions to represent leaking Hanford tank waste (Table 1). The composition of the STW solutions was based on data presented by Serne et al. (1998). Hanford tank waste has a very complex chemistry, and only the major chemical constituents were included in our study to keep the experimental system simple. The NaOH concentration was varied in the first two STWs (STW1 and STW2), while the Al concentration was constant. The STW3 solution consisted of a mixture of NaOH and $NaNO_3$, and was most representative of S-SX tank waste. All chemicals used were analytical grade; $NaAlO_2$ was obtained from Strem Chemicals; NaOH and $NaNO_3$ from Fisher Scientific; and $Al(NO_3)_3$ from Aldrich.

Batch Reaction Experiments

Hanford sediments were reacted with STW to mimic a Hanford tank leak. We reacted 100 g of Hanford sediments (<2-mm diam.) with 100 mL STW1 and STW2 in capped 250-mL polyethylene bottles for 1, 10, 25, and 50 d at two different temperatures (25 and 50°C) in a water bath. For STW3, 1 kg of sediment and 1 L of STW3 in capped 2-L polyethylene bottles were place in a 50°C electric oven for 25 and 40 d. To minimize abrasion, bottles were gently mixed by hand in an orbital motion once a day.

After the specified time periods (Table 1), sediments and liquids were separated by centrifugation (27 200 g for 60 min). Supernatant solution was transferred into polypropylene bottles, sealed with a screw cap, and kept at room temperature. The 50°C samples were diluted before cooling to room temperature to prevent precipitation of solids.

The solid materials were washed four times with deionized water and centrifuged. Colloidal particles with equivalent spherical diam. < 2 μm (assuming a 2.65 g cm^{-3} particle density) were fractionated by gravity sedimentation and dialyzed against deionized water until the electric conductivity was <0.01 dS m^{-1}. The suspended colloidal material was stored in polyethylene bottles.

Supernatant and Colloid Characterization

For the first two batch studies (STW1, STW2), Si and Al in the supernatant solutions were measured colorimetrically (Koroleff, 1983; Bertsch and Bloom, 1996). For the STW3 reactions, we measured Al, Si, Fe, K, Ca, and Mg in the supernatant by ICP–AES (Thermo Jarrell Ash IRIS ICP–AES, Thermo Electron Corporation, Waltham, MA) and Na by atomic absorption spectrophotometry (Varian 220 Flame Atomic Absorption Spectrometer, Varian Ltd., Mulgrave, Australia). Noncarbonate alkalinity (NCA) and carbonates were determined by titration (Jenkins et al., 1976). The NCA is reported as "14-pNCA" to use the same scale as pH. Nitrate was measured with an ion-selective electrode.

The colloidal fraction was characterized as follows. X-ray diffraction was performed with randomly oriented colloidal material on a glass XRD slide using Cu-Kα radiation (Philips XRG 3100, Philips Analytical, Inc., Mahwah, NJ) with scanning rates of 0.02° 2θ. The XRD patterns were obtained for Na-saturated samples, K-saturated (25 and 550°C), Mg-saturated, and Mg-glycerol saturated samples. The FTIR analysis was only obtained on the STW3 products. Colloidal material was pressed into KBr pellets (1% w/w) and analyzed using a PerkinElmer 2000 FTIR spectrometer (Wellesley, MA). Solid samples were also examined using SEM (Hitachi S570, Hitachi Limited, Tokyo, Japan) and EDAX. Electron micrographs were scanned optically to ensure representative images. Solid-state MAS-NMR spectra were recorded using an Avance 600 spectrometer (Bruker, Germany) at 14.09 T. Samples were packed into 2.5- and 4.0-mm rotors and measured at 119.217 and 156.375 MHz for ^{27}Al and ^{29}Si, respectively. For ^{27}Al-NMR, pulse duration was 0.75 μs, pulse delay was 6.0 s, and spinning rate was 35 kHz. For ^{29}Si-NMR measurements, pulse duration was 5.8 μs, pulse delay was 10.0 s, and spinning rate was 15 kHz. No cross-polarization was used for ^{29}Si NMR. Chemical shifts were expressed relative to the standard samples of $Al(NO_3)_3$ and tetramethylsilane for ^{27}Al and ^{29}Si, respectively.

The colloidal fraction was further treated with a 0.2 *M* acidic (pH 3) ammonium oxalate (AAO) solution to extract poorly crystalline precipitates (Smith and Mitchell, 1987) and labile aluminosilicates (Chorover et al., 2003). For these extractions,

Table 1. Simulated tank waste (STW) solutions, prepared at room temperature (20 to 22°C), and experimental conditions of batch experiments.

Designation of solution	NaOH	$NaAlO_2$	$Al(NO_3)_3$	$NaNO_3$	pH	Density (20°C)	Temperature†	Time†
	mol kg^{-1}					kg L^{-1}	°C	d
Control‡	0	0	0	0	7.1	0.99	50	25, 40
STW1	0.1	0	3.7×10^{-3}	0	13.0§	0.99	25, 50	1, 10, 25, 50
STW2	0.5	0	3.7×10^{-3}	0	13.7§	1.00	25, 50	1, 10, 25, 50
STW3	1.4	0.125	0	3.7	14.2§	1.20	50	25, 40

† Temperature and duration of batch reactions with sediments.
‡ Distilled water.
§ Determined by titration, which measures noncarbonate alkalinity (NCA), values reported are 14-pNCA [= 14 + $\log_{10}$(NCA)] to retain the same scale as pH.

Reproduced from Soil Science Society of America Journal. Published by Soil Science Society of America. All copyrights reserved.

the colloid suspension was shaken on a reciprocal shaker for 4 h in the dark. The supernatant solution obtained after centrifugation was acidified to pH ≈ 1. Aluminum, Si, and Mg in the supernatant were determined by ICP–AES. The solid material was examined by XRD as described above.

RESULTS AND DISCUSSION

Solution Characterization

Under STW2 (0.5 *M* NaOH), Al and Si concentrations in the supernatant solutions initially increased and reached a maximum between 1 and 25 d of reaction time, after which the concentrations decreased (Fig. 1). Higher reaction temperatures resulted in greater dissolved Al and Si concentrations. The AAO extractions indicate that a portion of the Si, Al, and Mg was incorporated into poorly crystalline or labile solids at both temperatures (25 and 50°C). The amount of labile solids increased initially and reached maximum values within the first 25 d of reaction.

In sediments treated with STW1 (0.1 *M* NaOH), dissolved Al concentrations steadily decreased and Si concentrations were relatively constant and much lower than under 0.5 *M* NaOH, a result similar to that reported by Kaplan et al. (1998). The solution alkalinity (14-pNCA) decreased as the Si concentration increased (Fig. 1), indicating the dissolution of silicate minerals. After the initial drop, the NCA remained constant, likely because of the high NaOH concentration and the buffering effect of Si dissolution and precipitation of new solid phases.

Higher OH and Al concentration (STW3) further increased Si release from the sediments (Table 2). Increased Si release is caused by elevated OH, but not by the elevated Al concentration, because Al decreases free OH concentrations through formation of $Al(OH)_4^-$ and thereby inhibits mineral dissolution (Qafoku et al., 2003b).

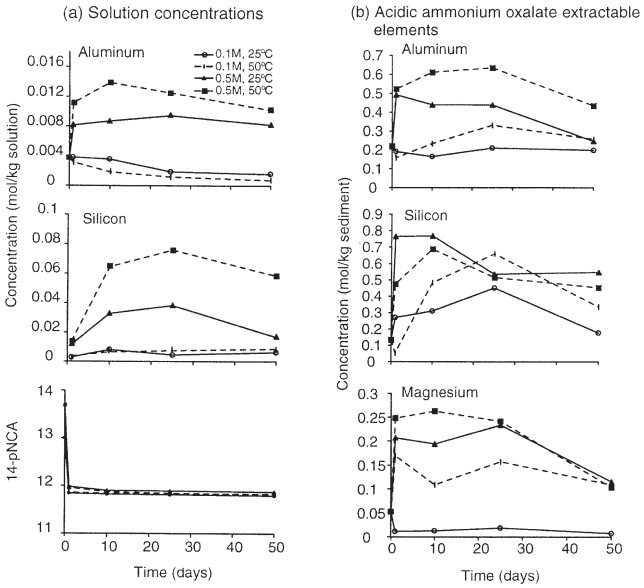

Fig. 1. (a) Chemical composition of the supernatant solution for STW1 (0.1 *M* NaOH) and STW2 (0.5 *M* NaOH) reactions as a function of time, and (b) acidic ammonium oxalate extractable Al, Si, and Mg from colloidal reaction products. 14-pNCA is noncarbonate alkalinity at the same scale as pH.

Silica concentrations in solution decreased slightly between 25 and 40 d of reaction time, similar to the results from the lower OH treatments (Fig. 1 and Table 2). Only a small fraction of the Al initially added to the solutions remained in the supernatant solution (Table 2). The AAO extracts showed no differences in the amount of poorly crystalline solids between 25 and 40 d of reaction time, indicating no obvious change in lability and/or quantity of the solids precipitated during this time interval (data not shown).

The results of our study are similar to the ones reported by Qafoku et al. (2003b), who also observed an initial increase in Si concentration, followed by a decrease after about 3 d of reaction time, when Hanford sediments were contacted with alkaline tank waste simulants. The decrease in Si concentrations was also attributed to precipitation of secondary phases (Qafoku et al., 2003a, 2003b).

Colloid Formation and Characterization

X-Ray Diffraction

The untreated Hanford sediments contain four major layered clay minerals—chlorite, smectite, kaolinite, and illite—and primary minerals mica, quartz, christobalite, albite, and microcline (Fig. 2). Figure 2 also shows the XRD patterns of the colloidal material obtained with 0.1 and 0.5 *M* NaOH solutions at 50°C. No new mineral phases were detected by XRD. We observed that the diffraction peak at *d*-spacing 0.142 nm broadened and shifted to 0.147 nm after 1 d of reaction for both 0.1 and 0.5 *M* NaOH treatments. This peak disappeared following extraction with AAO (Fig. 3), which suggests that the peak is caused by minerals that dissolve in AAO. We believe that the peak is caused by hydroxy-interlayering of Al, Si, and Mg in chlorite and/or smectite. No shift in the 0.142-nm peak occurred in the XRD pattern of colloids from untreated sediment when extracted with AAO, indicating that the interlayered material formed as a result of the STW treatment.

To investigate relative peak differences of the untreated and treated Hanford sediments, we normalized the XRD intensities of kaolinite and illite (Na-saturated) with respect to the intensity of quartz (at 0.34 nm) (Table 3). The ratio of the intensities of kaolinite to quartz was fairly constant across time in the products of the 0.1 and 0.5 *M* NaOH treatments; however, the illite to quartz ratio increased over time. This indicates that the relative abundance of illite compared with quartz and kaolinite increases with time. It seems that quartz and kaolinite are dissolving at a higher rate than illite, leading to a relatively more pronounced illite XRD peak.

As NaOH concentration increased, the relative peak intensities of kaolinite and illite decreased relative to quartz (Table 3) and, at the highest NaOH concentration (1.68 *M*), new peaks characteristic of the feldspathoids NO_3–cancrinite and NO_3–sodalite (Buhl et al., 2000; Buhl, 1991) and zeolite A (Wyckoff, 1968) appeared (Fig. 2c). Zeolite seemed not to be stable in this system and disappeared after 40 d of reaction time (Fig. 3b).

Reproduced from Soil Science Society of America Journal. Published by Soil Science Society of America. All copyrights reserved.

Table 2. Measured chemical composition of the supernatant solution (STW3) at 50°C.

Supernatant	Al	Ca	Fe	K	Mg	Si	Na	NO_3	CO_3	pH
	mol kg^{-1}									
				25 d of reaction time						
Control	0	0.6375	0	0.0001	0.0001	0.001	0	0	0	7.1
STW3	0.0008	0	0.0004	0.028	2.5×10^{-5}	0.301	2.481	1.606	0.0274	13.8†
				40 d of reaction time						
Control	0	0.6329	0	0.0001	0.0001	0.001	0	0	0	7.9
STW3	0.0015	5.3×10^{-5}	0.0035	0.030	8.4×10^{-6}	0.252	2.542	2.064	0.0274	13.8†

† Determined by titration which measures noncarbonate alkalinity (NCA). Values reported are 14 + $\log_{10}$(NCA) to maintain the same scale as pH.

Treatment of the reacted sediments with AAO removed the zeolite peak, and the sodalite and cancrinite peaks weakened. This indicates that these new phases are labile phases in the presence of AAO (pH = 3) (Fig. 3b). The XRD intensities of the new minerals (cancrinite and sodalite) relative to quartz increased with time for STW3 (25 to 40 d), indicating that the new minerals are more stable than quartz (Table 3). At the same time, a decrease in the kaolinite/quartz relative intensity suggests that the formation of zeolite, cancrinite, and sodalite enhanced the dissolution of kaolinite by removing Al from solution.

For all treatments (0.1, 0.5, and 1.68 *M* NaOH), the supernatant compositions and XRD patterns indicate enhanced desilication along with the alteration of preexisting colloidal silicates. Increasing NaOH concentrations resulted in a reduction of the quartz and feldspar peaks along with a relative change in the aluminosilicate mineral peaks. Illite seemed to be more resistant toward alkaline treatment than kaolinite. Kaolinite is known to

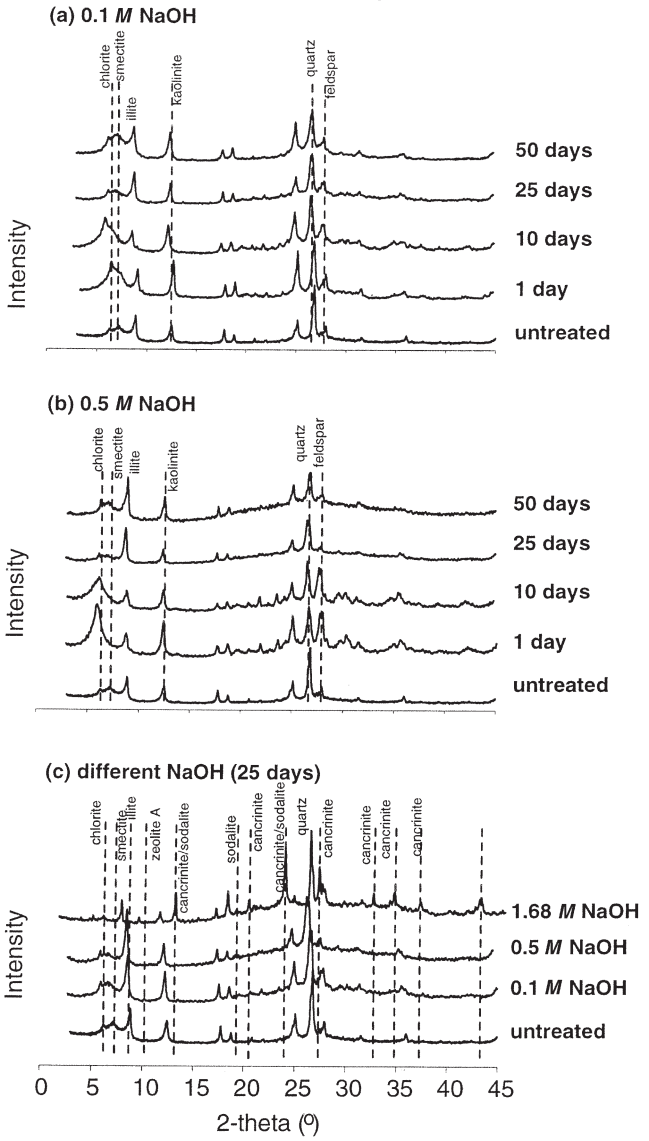

Fig. 2. X-ray diffraction patterns of Na-saturated colloidal material extracted from Hanford sediments reacted with simulated tank waste solutions at 50°C; (a) and (b) show the effect of reaction time on mineral alteration, and (c) shows the effect of NaOH concentrations on mineral alterations.

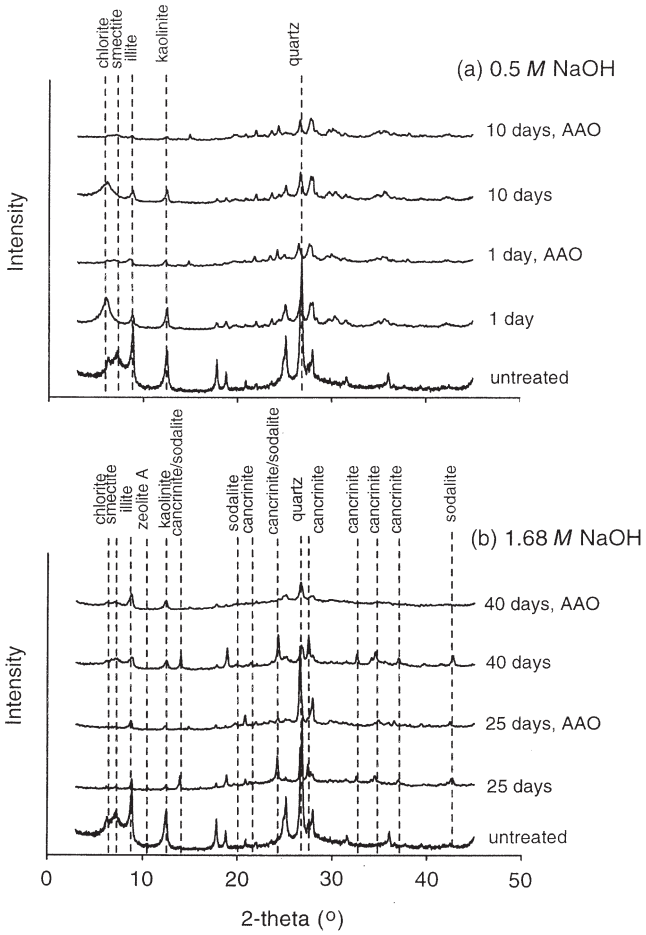

Fig. 3. X-ray diffraction patterns of Na-saturated colloidal material extracted from Hanford sediments reacted with simulated tank waste solutions at 50°C. Patterns are shown for colloids before and after acidic ammonium oxalate (AAO) extraction.

Reproduced from Soil Science Society of America Journal. Published by Soil Science Society of America. All copyrights reserved.

Table 3. Relative XRD intensities of kaolinite (K), illite (I), cancrinite (C), and sodalite (S) with respect to quartz (Q) for simulated tank wastes STW1 (0.1 *M* NaOH), STW2 (0.5 *M* NaOH), and STW3 (1.68 *M* NaOH).

	0.1 *M* NaOH		0.5 *M* NaOH		1.68 *M* NaOH			
Reaction time	K/Q	I/Q	K/Q	I/Q	K/Q	I/Q	C/Q	S/Q
d								
0 (untreated)	0.48	0.32	0.48	0.32	0.48	0.32	0	0
1	0.64	0.49	0.65	0.46	nd†	nd	nd	nd
10	0.48	0.39	0.50	0.45	nd	nd	nd	nd
25	0.45	0.59	0.48	0.68	0.14	0.28	0.63	0.20
50/40	0.56‡	0.66‡	0.57‡	0.64‡	0.31§	0.41§	0.90§	0.23§

† nd, not determined.
‡ 50 d of reaction time.
§ 40 d of reaction time.

be labile in NaOH solutions (e.g., Barrer, 1982; Chorover et al., 2003; Zhao et al., 2004). In contrast to kaolinite, smectite appeared fairly resistant to dissolution by STW solutions. The difference in behavior between the two kinds of minerals (1:1 and 2:1) can be explained by structural differences. For kaolinite, hydrolysis of the tetrahedral and octahedral sheets occurs as simultaneous dissolution reactions, and the rate-limiting step is the dissolution of the octahedral layer. In smectite, dissolution occurs as serial reactions, where dissolution of the tetrahedral layer is the rate-limiting step (Bauer and Berger, 1998). Smectite, however, is still susceptible to dissolution in alkaline Hanford tank waste, and its dissolution contributes to the Si concentration in solution (Qafoku et al., 2003a).

Fourier Transform Infrared Spectra

The FTIR spectra of the products of the 1.4 *M* NaOH treatment substantiate the results obtained from the XRD patterns (Fig. 4). The absorption bands in the midinfrared indicate the alteration of original clay minerals and the formation of new phases. We notice that the intensities of the kaolinite bands at 3696 and 3620 cm^{-1} remain, but relative to the Si–O–Al stretch near 1000 cm^{-1}, these band intensities decreased with time. The absorption bands for the 25-d spectrum show the asymmetric and symmetric vibration modes within the fingerprint area of tectosilicates (400–800 cm^{-1}). The characteristic bands occur for sodalite at ≈668 and 730 cm^{-1}, for cancrinite at ≈512, 571, 619, and 682 cm^{-1} (Barnes et al., 1999), and for zeolite A at ≈668 and 462 cm^{-1} (Aronne et al., 2002). The asymmetric stretching vibrations at 1011, 1081, and 1163 cm^{-1} were shifted to a broad band centered near 999 cm^{-1}. This band supports the presence of tectosilicates containing tetrahedral SiO_4 and AlO_4. Main absorption bands occur at 999 cm^{-1} for zeolite A (Aronne et al., 2002), at 1095, 1035, and 979 cm^{-1} for cancrinite, and at 979 cm^{-1} for sodalite (Zheng et al., 1997). The results after 40 d of reaction time indicate the presence of cancrinite and sodalite, but there is no evidence for zeolite A. The narrowing of the Si–O–Al stretch near 1000 cm^{-1} suggests increasing crystallinity and/or homogeneity of the products, consistent with the XRD patterns and AAO extractions.

For both reaction times (25 and 40 d), the sharp FTIR absorption bands at 1423 and 1383 cm^{-1} indicate the enclathration of nitrate within the cancrinite (Buhl et al., 2000) and sodalite cages (Buhl and Löns, 1996). This nitrate was not sorbed or precipitated at the mineral surface, as we had extensively washed and dialyzed the samples with water. No evidence was found for enclathration of carbonate, which would have characteristic bands at 1410 and 1455 cm^{-1} (Hackbarth et al., 1999; Barnes et al., 1999).

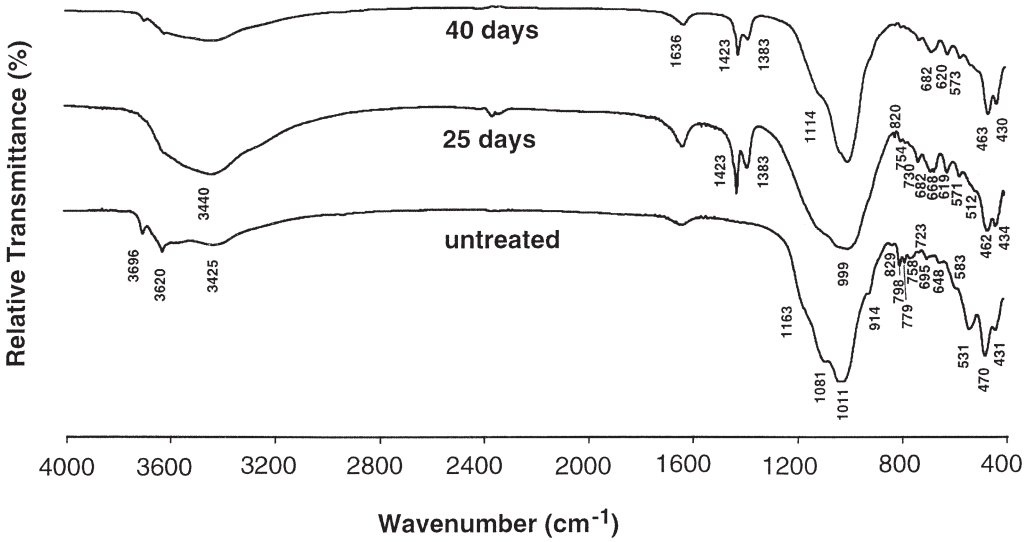

Fig. 4. Fourier transform infrared spectra of Hanford sediments reacted with simulated tank waste (STW3, 1.68 *M* NaOH) at 50°C.

Reproduced from Soil Science Society of America Journal. Published by Soil Science Society of America. All copyrights reserved.

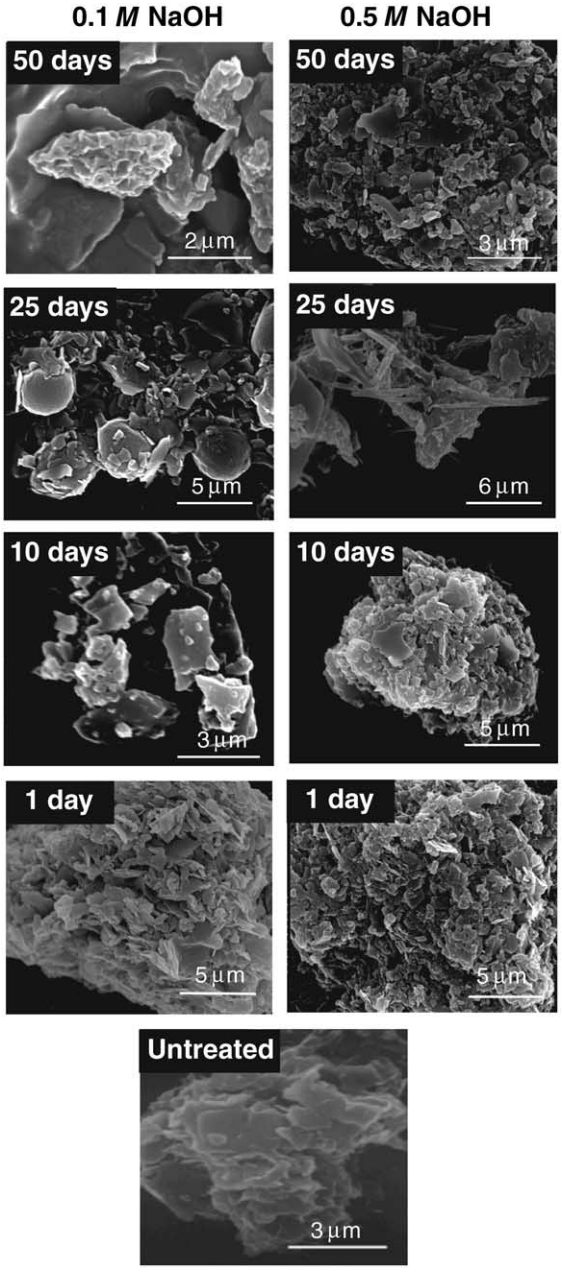

Fig. 5. Scanning electron micrographs of Hanford sediments reacted with simulated tank waste STW1 (0.1 *M* NaOH) and STW2 (0.5 *M* NaOH) at 50°C.

The characteristic peak at 1636 cm^{-1} for the water bending vibration became less pronounced relative to the Si–O–Al stretch with increasing reaction time (Fig. 4). This implies an increase of bonded OH^- in the crystal structure. Parallel to the increased amount of OH^-, the amount of NO_3^- inside the structure decreased with time. The intensity of the two nitrate absorption bands (1423 and 1383 cm^{-1}) also decreased with time, indicating the loss of NO_3^- from the framework. Within the same time interval, we observed an increase in NO_3^- in the solution phase (Table 2).

The XRD, FTIR, and AAO extracts indicate that there was an increase in the crystallinity of the new solid phases, sodalite and cancrinite, between 25 and 40 d. The simultaneous loss of nitrate from the solid phases indicates that these more crystalline phases enclathrate less nitrate into their structures. Cancrinite has both cages and channels (Gerson and Zheng, 1997), whereas sodalite (Gerson and Zheng, 1997) and zeolite A (Aronne et al., 2002) have a series of interlocking cages. The wide channel in the cancrinite is filled with cations and intracrystalline anions such as CO_3 or NO_3, whereas the small cages contain only cations and water molecules (Hackbarth et al., 1999; Buhl et al., 2000). Bickmore et al. (2001) suggested that defects in the cancrinite structure could close channel access to the bathing solution. Such defects could account for more trapped nitrate in the less-crystalline phases formed at 25 d.

Colloid Morphology

The distinct morphology of the native clay minerals, illite, smectite, and kaolinite can be seen in the colloidal fraction of the untreated Hanford sediment (Fig. 5). The sediments treated with 0.1 and 0.5 *M* NaOH show alteration of the native clay minerals as a result of mineral dissolution. The most pronounced change occurred after 25 d, when spherical particles appeared in the 0.1 *M* NaOH treatment and rod-shaped particles in the 0.5 *M* NaOH treatment. The EDAX results showed that the spherical particles consisted dominantly of Fe, whereas the rod-shaped particles contained Al, Si, Mg, and Fe. Both particle types were labile (or metastable) and disappeared after 50 d of reaction time. Iron-rich precipitates were also observed by others when Hanford sediments were contacted with 1 mol L^{-1} NaOH solutions (Qafoku et al., 2003a). The SEM photographs for STW3 showed a pronounced change in the morphology of the original clay minerals: spherical, cauliflower-like, and rod-shaped particles with surface features common to sodalite and cancrinite appeared. These morphological changes indicate the formation of neophases at the expense of the original clay minerals as a result of secondary nucleation.

Structural Characterization with ^{27}Al and ^{29}Si NMR

The ^{27}Al-NMR spectra of the untreated colloidal materials have two intense peaks at chemical shifts of 59.7 and 4.1 ppm (Fig. 6), representing four and six-coordinated Al, respectively (Wilson, 1987). Little change was observed in the NMR spectrum of 0.1 *M* NaOH samples compared with untreated sediment. For the 0.5 *M* NaOH treatment, the intensity of the Al(4) peak increased relative to the Al(6) peak at the beginning then decreased after 10 d. We interpret the initial decrease in the Al(6)/Al(4) ratio as due to dissolution of clay minerals, primarily kaolinite. The subsequent increase in this ratio probably reflects the rates of quartz and feldspar dissolution relative to kaolinite dissolution (Fig. 2 and Table 3) and to precipitation of poorly crystalline aluminosilicates as indicated by the increase in AAO-extractable Al in Fig. 1. At a higher NaOH concentration (1.68 *M*), the Al coordination changed from octahedral to tetrahedral (Fig. 6c), again consistent with the formation of tectosilicate minerals.

Reproduced from Soil Science Society of America Journal. Published by Soil Science Society of America. All copyrights reserved.

Untreated Hanford sediments showed a major ^{29}Si NMR resonance at −91.8 ppm and a minor resonance at −105.7 ppm (Fig. 7). Kaolinite has a resonance at −92.1 ppm, illite at −91.0 ppm (Kinsey et al., 1985), and crystalline SiO_2 at −105.7 ppm (Wilson, 1987). The chemical shift for Si becomes less negative when Si is shielded by increasing Al(4) concentration in the structure (Kinsey et al., 1985). In both the 0.1 and 0.5 *M* NaOH treatments, the resonance near −91.8 ppm shifts toward −92.6 ppm, indicating increased Si polymerization and Al-shielding as network aluminosilicates begin to form and phyllosilicates are dissolved. Neither of these treatments resulted in obvious changes in the ^{27}Al-NMR spectra or XRD diffractograms; ^{29}Si-NMR is evidently more sensitive to changes occurring at lower NaOH concentration. Increasing the alkalinity to 1.68 *M* NaOH resulted in a more pronounced chemical shift of the −91.8 ppm peak to −87.3 ppm characteristic of Si(4Al) units in cancrinite and sodalite (Buhl, 1991; Buhl et al., 2000).

The NMR results provide further evidence that native minerals (octahedral Al) are dissolved and zeolite and feldspathoids (tetrahedral Al and increasing Al/Si disorder) are forming. The NMR results corroborate the results obtained by XRD and FTIR, and provide semiquantitative information regarding the relative abundance of Al(4) and Al(6). Furthermore, the chemical shifts indicate changes in short range ordered minerals and are more sensitive to the overall Si and Al transformations than XRD or FTIR.

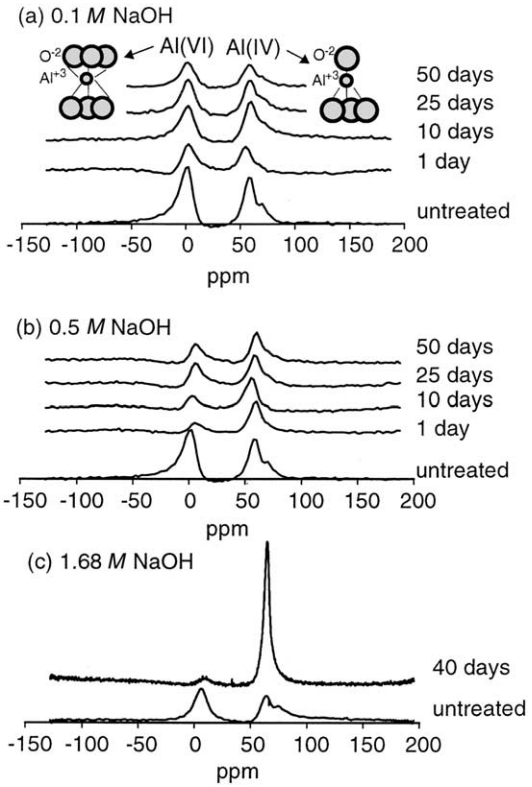

Fig. 6. ^{27}Al NMR of unreacted and reacted Hanford sediments at 50°C. (a) NMR spectra for 0.1 *M* NaOH, (b) NMR spectra for 0.5 *M* NaOH, and (c) NMR spectra for 1.68 *M* NaOH.

CONCLUSIONS

Leaking tank solutions at the Hanford Reservation can alter the mineralogical composition of vadose zone sediments. First, Si is released from the native minerals and second, new minerals precipitate. Both processes are enhanced as temperature and NaOH concentration are increased. At high NaOH concentration (1.68 *M* NaOH), we observed the formation of three new minerals: NO_3–cancrinite, NO_3–sodalite, and zeolite A. Zeolite A was less stable than cancrinite and sodalite. The dissolution and precipitation reactions occurred during time scales of several days, with dissolution of kaolinite dominating initially and precipitation of feldspathoids dominating in the later stages. At lower alkalinity (<0.5 *M* NaOH), there is evidence that poorly crystalline materials precipitated, likely hydroxy-interlayer Mg, Al, and Si in the existing 2:1 layered clay minerals. Portions of the dissolved Si, Al, and Mg were incorporated into poorly crystalline solids. Kaolinite and quartz were both more labile relative to illite during 40 to 50 d of reaction time.

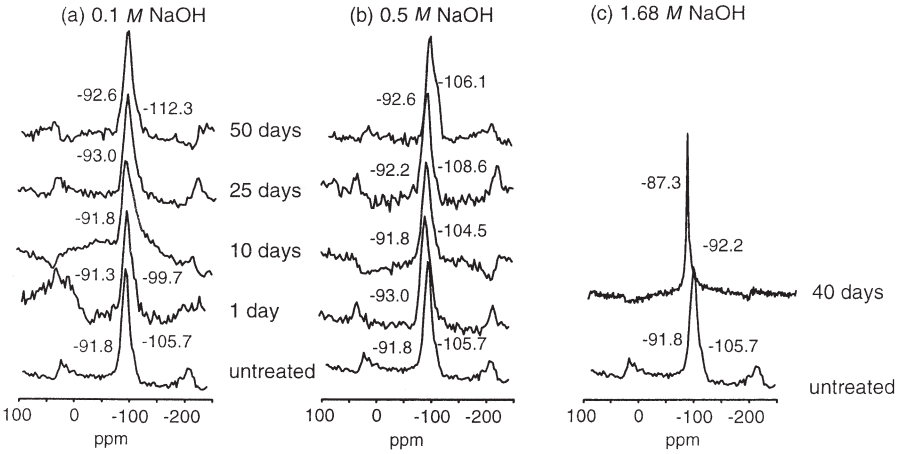

Fig. 7. ^{29}Si NMR of unreacted and reacted Hanford sediments at 50°C. (a) 0.1 *M* NaOH, (b) 0.5 *M* NaOH, and (c) 1.68 *M* NaOH. Numbers indicate major chemical shifts with respect to tetramethylsilane.

Reproduced from Soil Science Society of America Journal. Published by Soil Science Society of America. All copyrights reserved.

ACKNOWLEDGMENTS

This research was supported by the Office of Science (BER), U.S. Department of Energy, Grant No. DE-FG07-99ER62882. We thank Jeff Boyle and Hongting Zhao for help with the experiments, the Electron Microscopy Center at WSU for use of their facility, Dan Mitchell (Center for NMR Spectroscopy at WSU) for the NMR work, Dan Strawn (University of Idaho) for the use of FTIR equipment, and John Zachara and Jeff Serne (Pacific Northwest National Laboratory) for providing us with the Hanford sediments. The WSU NMR Center equipment was supported by NIH grants RR0631401 and RR12948, NSF grants CHE-9115282 and DBI-9604689 and the Murdock Charitable Trust.

REFERENCES

Aronne, A., S. Esposito, C. Ferone, M. Pansini, and P. Pernice. 2002. FTIR study of the thermal transformation of barium-exchanged zeolite A to celsian. J. Mater. Chem. 12:3039–3045.

Barnes, M.C., J. Addai-Mensah, and A.R. Gerson. 1999. The mechanism of the sodalite-to-cancrinite phase transformation in synthetic spent Bayer liquor. Microporous Mesoporous Mater. 31:287–302.

Barrer, R.M. 1982. Hydrothermal chemistry of zeolites. Academic Press, London.

Bauer, A., and G. Berger. 1998. Kaolinite and smectite dissolution rate in high molar KOH solutions at 35° and 80°C. Appl. Geochem. 13:905–916.

Bauer, A., and B. Velde. 1999. Smectite transformation in high molar KOH solutions. Clay Miner. 34:259–273.

Bertsch, P.M., and P.R. Bloom. 1996. Aluminum. p. 517–550. *In* D.L. Sparks (ed.) Methods of soil analysis: Part 3—Chemical methods. SSSA Book Ser. No. 5. SSSA and ASA, Madison, WI.

Bickmore, B.R., K.L. Nagy, J.S. Young, and J.W. Drexler. 2001. Nitrate-cancrinite precipitation on quartz sand in simulated Hanford tank solutions. Environ. Sci. Technol. 35:4481–4486.

Buhl, J.C. 1991. The properties of salt-filled sodalites. Part 2. Synthesis, decomposition reactions and phase transitions of nitrate sodalite, $Na_8[AlSiO_4]_6(NO_3)_2$. Thermochim. Acta 189:75–82.

Buhl, J.C., W. Hoffmann, W.A. Buckermann, and W. Müller-Warmuth. 1997. The crystallization kinetics of sodalites grown by the hydrothermal transformation of kaolinite studied by ^{29}Si MAS NMR. Solid State Nucl. Magn. Reson. 9:121–128.

Buhl, J.-C., and J. Löns. 1996. Synthesis and crystal structure of nitrate enclathrated sodalite $Na_8[AlSiO_4]_8(NO_3)_2$. J. Alloys Comp. 235:41–47.

Buhl, J.C., F. Stief, M. Fechtelkord, T.M. Gesing, U. Taphorn, and C. Taake. 2000. Synthesis, x-ray diffraction and MAS NMR characteristics of nitrate cancrinite $Na_7[AlSiO_4]_6(NO_3)_{1.6}(H_2O)_2$. J. Alloys Comp. 305:93–102.

Chorover, J., S. Choi, M.K. Amistadi, K.G. Karthikeyan, G. Crosson, and K.T. Mueller. 2003. Linking cesium and strontium uptake to kaolinite weathering in simulated tank waste leachate. Environ. Sci. Technol. 37:2200–2208.

Cuadros, J., and J. Linares. 1996. Experimental kinetic study of the smectite-to-illite transformation. Geochim. Cosmochim. Acta 60: 439–453.

Gephart, R.E., and R.E. Lundgren. 1998. Hanford tank cleanup: A guide to understanding the technical issues. 4th ed. Battelle Press, Columbus.

Gerson, A.R., and K. L. Zheng. 1997. Bayer process plant scale: Transformation of sodalite to cancrinite. J. Crystal Growth 171:209–218.

Hackbarth, K., T.M. Gesing, M. Fechtelkord, F. Stief, and J.C. Buhl. 1999. Synthesis and crystal structure of carbonate cancrinite $Na_8[AlSiO_4]_6CO_3(H_2O)_{3.4}$ grown under low-temperature hydrothermal conditions. Microporous Mesoporous Mater. 30:347–358.

Jenkins, D., V.L. Snoeyink, J.F. Ferguson, and J.O. Leckie. 1976. Water chemistry laboratory manual. Association of Environmental Engineering Professors.

Kaplan, D.I., K.E. Parker, and J.C. Ritter. 1998. Effects of aging quartz sand and Hanford sediment with sodium hydroxide on radionuclide sorption coefficients and sediment physical and hydrologic properties: Final report for Subtask 2a. Pacific Northwest National Laboratory, USDOE, Richland, WA.

Kinsey, R.A., R.J. Kirkpatrick, J. Hower, K.A. Smith, and E. Oldfield. 1985. High resolution aluminum-27 and silicon-29 magnetic resonance spectroscopic study of layer silicates, including clay minerals. Am. Mineral. 70:537–548.

Koroleff, F. 1983. Determination of silicon. p. 174–183. *In* K. Grasshoff et al. (ed.) Methods of seawater analysis. Verlag Chemie, Weinheim.

Mashal, K., J.B. Harsh, M. Flury, A.R. Felmy, and H. Zhao. 2004. Colloid formation in Hanford sediments reacted with simulated tank waste. Environ. Sci. Technol. 38:5750–5756.

Nyman, M., J.L. Krumhansl, P. Zhang, H. Anderson, and T.M. Nenoff. 2000. Chemical evolution of leaked high-level liquid wastes in Hanford soils. Mater. Res. Soc. Symp. Proc. 600:225–230.

Park, M., C.L. Choi, W.T. Lim, M.C. Kim, J. Choi, and N.H. Heo. 2000. Molten-salt method for the synthesis of zeolitic materials: I. Zeolite formation in alkaline molten-salt system. Microporous Mesoporous Mater. 37:81–89.

Pruess, K., S. Yabusaki, C.I. Steefel, and P.C. Lichtner. 2002. Fluid flow, heat transfer, and solute transport at nuclear waste storage tanks in the Hanford vadose zone. Available at www.vadosezonejournal.org. Vadose Zone J. 1:68–88.

Qafoku, N.P., C.C. Ainsworth, J.E. Szecsody, D. Bish, J.S. Young, D.E. McCready, and O.S. Qafoku. 2003a. Aluminum effect on dissolution and precipitation under hyperalkaline conditions: II. Solid phase transformations. J. Environ. Qual. 32:2364–2372.

Qafoku, N.P., C.C. Ainsworth, J.E. Szecsody, and O.S. Qafoku. 2003b. Aluminum effect on dissolution and precipitation under hyperalkaline conditions: I. Liquid phase transformations. J. Environ. Qual. 32:2354–2363.

Qafoku, N.P., C.C. Ainsworth, J.E. Szecsody, and O.S. Qafoku. 2004. Transport-controlled kinetics of dissolution and precipitation in the sediments under alkaline and saline conditions. Geochim. Cosmochim. Acta 68:2981–2995.

Serne, R.J., R.E. Clayton, I.V. Kutnyakov, G.V. Last, V.L. LeGore, T.C. Wilson, H.T. Schaef, M.J. O'Hara, K.B. Wagnon, D.C. Lanigan, C.F. Brown, B.A. Williams, C.W. Lindenmeier, R.D. Orr, D.S. Burke, and C.C. Ainsworth. 2002. Characterization of vadose zone sediment: Borehole 41–09–39 in the S-SX Waste Management Area. No. PNNL-13757-3. Pacific Northwest National Laboratory, USDOE, Richland, WA.

Serne, R.J., J.M. Zachara, and D.S. Burke. 1998. Chemical information on tank supernatants, Cs adsorption from tank liquids onto Hanford sediments, and field observations of Cs migration from past tank leaks. No. PNNL-11495. Pacific Northwest National Laboratory, Richland, WA.

Smith, B.F.L., and B.D. Mitchell. 1987. Characterization of poorly ordered minerals by selective chemical methods. p. 275–299. *In* M.J. Wilson (ed.) A handbook of determinative methods in clay mineralogy. Chapman and Hall, New York.

Taubald, H., A. Bauer, T. Schäfer, M. Satir, and J.I. Kim. 2000. Experimental investigation of the effect of high-pH solutions on the Opalinus shale and the Hammerschmiede smectite. Clay Miner. 35:515–524.

Wilson, M.A. 1987. NMR techniques and applications in geochemistry and soil chemistry. Pergamon Press, Oxford.

Wyckoff, R.W.G. 1968. Crystall structures: Miscellaneous inorganic compounds, silicates, and basic structural information. Vol. 4. 2nd ed. John Wiley & Sons, New York.

Zhao, H., Y. Deng, J.B. Harsh, M. Flury, and J. Boyle. 2004. Alteration of kaolinite to cancrinite and sodalite by simulated Hanford tank wastes and its impact on cesium retention. Clays Clay Miner. 52: 1–13.

Zheng, K., A.R. Gerson, J. Addai-Mensah, and R.S.C. Smart. 1997. The influence of sodium carbonate on sodium aluminosilicate crystallization and solubility in sodium aluminate solutions. J. Crystal Growth 171:197–208.